CHAPTER V
RESULTS AND DISCUSSION

The experiment was performed at 800°C and both co-and counter-flow configurations were investigated. As mentioned previously in chapter II, the performance of SOFC is measured by I-V curve, a relation between current density (A/cm^2) and voltage (V). It is noted that, performances of both co- and counter-flows cannot be compared because the cell performances were gradually degraded everyday. This is due to a degradation of stainless anodic tube that supplies fuel to the cell. The similar report was also published by Marquez *et al.*, 2007. They found that after operating on syngas (H_2, N_2, CO and H_2O mixture), there was an effect not only in the cell, but also in the additional components of the stack, where the simultaneous injection of CO. Moreover, increased water content caused the system to degrade at a high rate.

5.1 Effect of Fuel Rate

The experimental cell performances for various fuel flow rates including both co- and counter-flows are illustrated in Fig. 5.1(a) and (b), respectively. Only H_2 was used as fuel and varied while air was kept as constant at 100 mL/min. Evidently, from Fig. 5.1, the cell performance is greater as increasing fuel flow rate due to a better supply to electrochemical reaction sites. Therefore, more current can be produced and a concentration polarization is decreased. The results also indicate that the OCV slightly increases at higher flow rates from 1.1 to 1.178 V for the co-flow and 1.099 to 1.176 V for the counter-flow. A similar effect was reported by Suwanwarangkul *et al.* 2006 and Cunningham *et al.*, 2004.

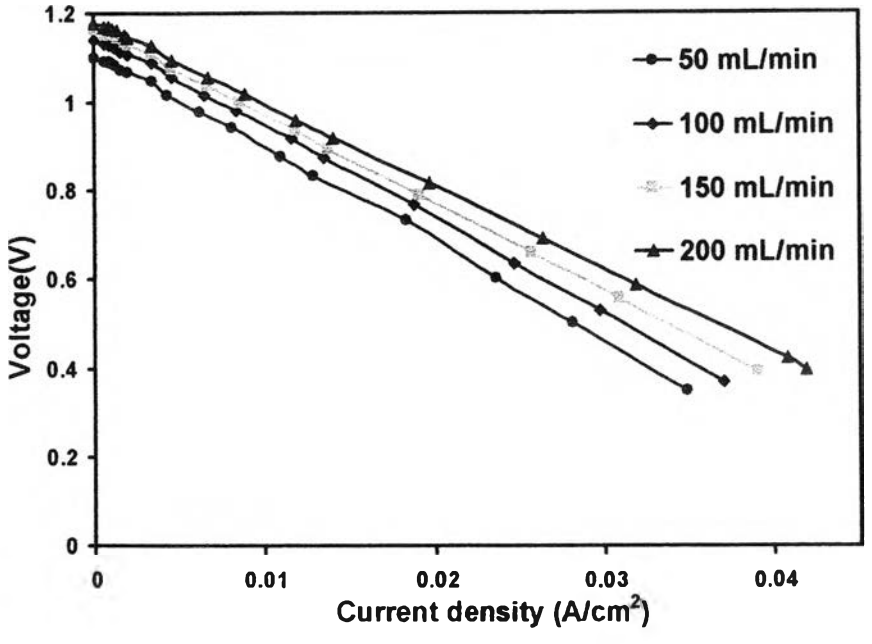

(a)

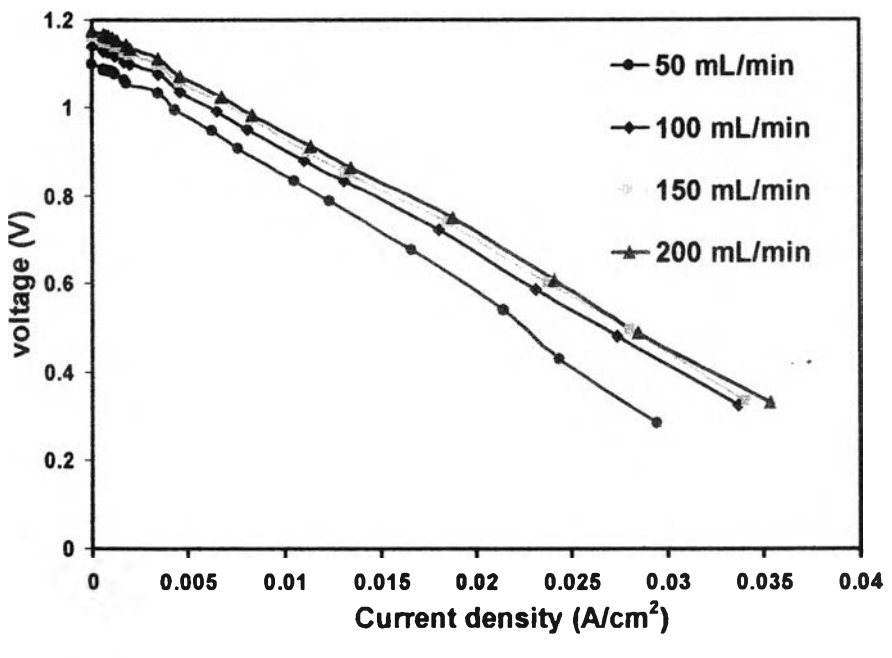

(b)

Figure 5.1 Experimental (a) co-flow and (b) counter-flow cell performances using various fuel flow rates.

5.2 Effect of Air Flow Rate

Fig. 5.2 shows the experimental cell performances of both co- and counter-flows for various air flow rates while fuel flow rate was kept as constant at 200 mL/min, and only H_2 was used as fuel. The results indicate that the air flow rate does

not affect to the cell performance. Therefore, the cell performances of both co- and counter-flows still give the same even operating at a higher air flow rate. This implies that at the lowest flow rate of 100 mL/min, O_2 is exceeding for an electrochemical reaction and air does not act as a cooling fluid since if it was, at higher flow rate, the cell performance would decrease because of a rising of activation and ohmic overpotentials due to a decrease of the cell temperature, resulting in a decrease in the cell performance. In contrast with Leng *et al.*, 2004, they found that at high current density, the air flow rate affected significantly to the cell performance.

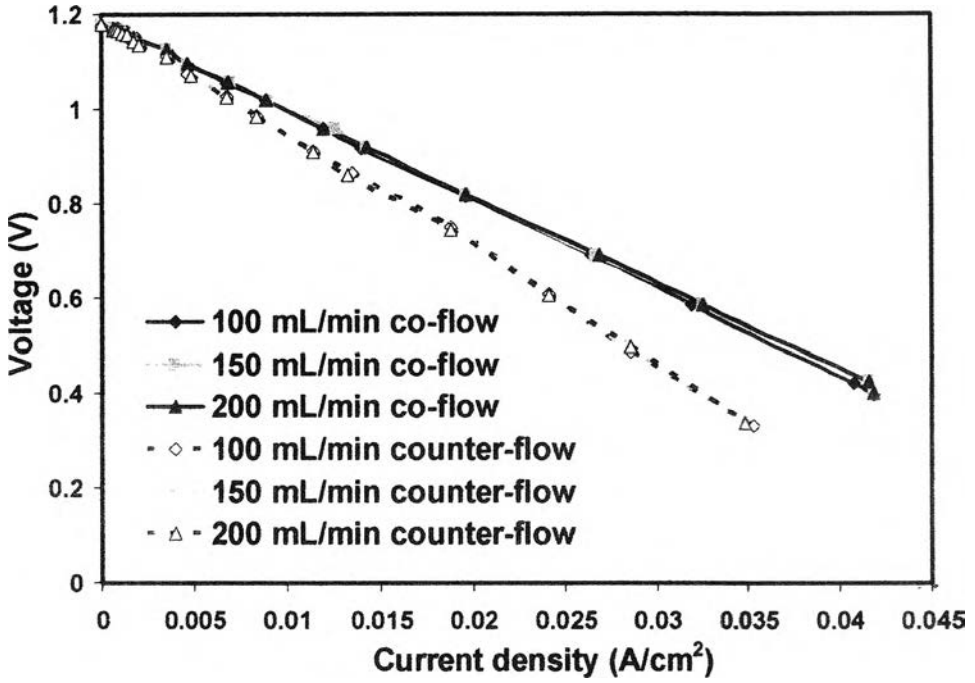

Figure 5.2 Experimental cell performances using various air flow rates for both co-and counter-flows

5.3 Effect of N_2 Dilution

A mixture of H_2+N_2 is used as fuel and fixed its flow rate of 200 mL/min in all cases. Figures 5.3 (a) and (b) show the experimental cell performances of various H_2+N_2 compositions for co-flow and counter-flow, respectively. From the figure a higher %N_2 causes a decrease in the cell voltage because the OCV decreases as a partial pressure of H_2 decreases, according to the Nernst's equation (Equation 2-6) derived from the thermodynamic aspect. Moreover, N_2 is acting as an inert gas that can retard the diffusion of H_2 from the bulk to an anode surface. Therefore, if a high

amount of N_2 is present, H_2 has less capability to evenly distribute over the entire electrode and to reaction sites. As a result, the cell performance is decreased with higher $\%N_2$ dilution. However, the impact of N_2 dilution is modest and the cell performance decreases about 29.8% for the co-flow and 35.3% for the counter-flow at 0.7 V when $\%N_2$ increases from 0 to 80% dilution. This result is coincided with Suwanwarangkul *et al.*

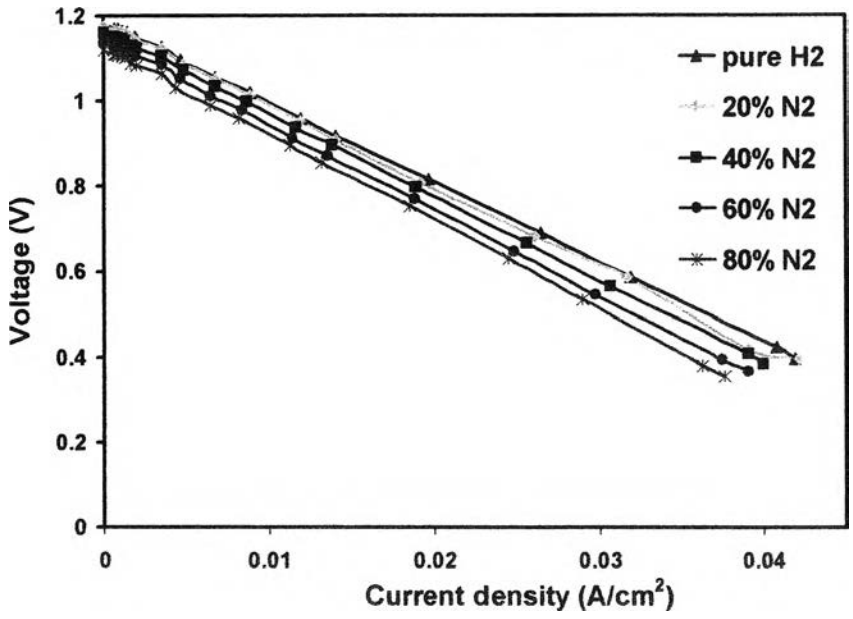

(a)

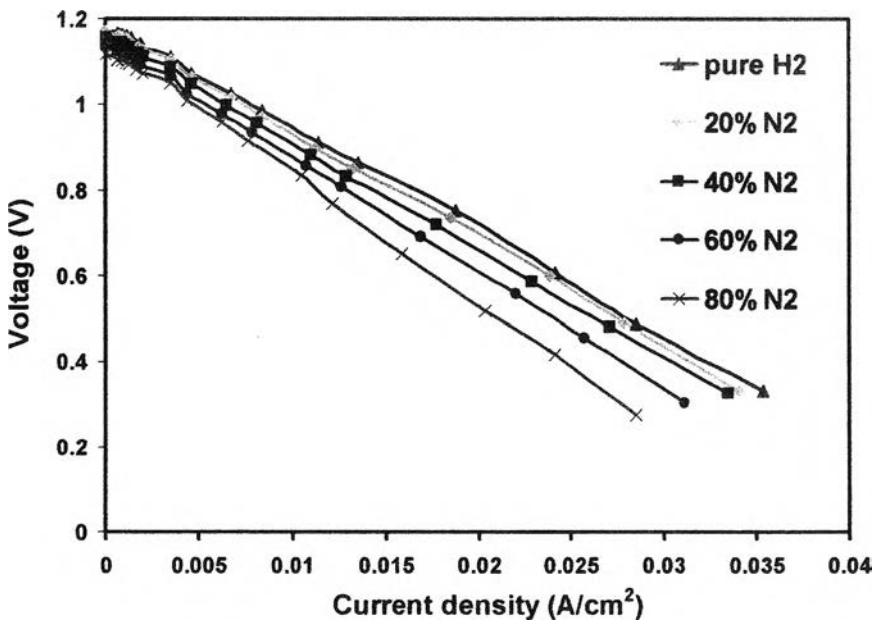

(b)

Figure 5.3 Experimental (a) co-flow and (b) counter-flow cell performances using various H_2+N_2 compositions.

5.4 Effect of CO_2 Dilution

Figures 5.4 (a) and (b) show the cell performances using various H_2+CO_2 compositions for both co- and counter-flows, respectively. A mixture of H_2+CO_2 was used as fuel and %CO_2 was varied up to 80%. The results of both co- and counter-flows imply that the effect of CO_2 dilution is greater than that of N_2 dilution because the cell performance with H_2+CO_2 is lower than that with H_2+N_2 for the same % dilution. Similar results were reported by Costa-nunes *et al*, 2005 and Jiang and Virkar, 2003. They found that the cell performance of CO+N_2 system was greater than CO+CO_2 system. In this case, at 0.7 V, the cell performance decreases about 74% for both co- and counter-flows when %CO_2 increases up to 80%. Moreover, the OCV of both co- and counter-flows significantly decrease about 25%. This is likely due to the impact of WGS reaction (Equation 2-4) which strongly influences the equilibrium composition of H_2+CO_2 mixture and is catalyzed by anodic Ni. The WGS reaction can convert H_2 and CO_2 back to H_2O and CO (Suwanwarangkul *et al.*, 2006.), leading to a less partial pressure of H_2 at anode, resulting in a lower OCV, according to Nernst's equation, and decreasing the cell performance.

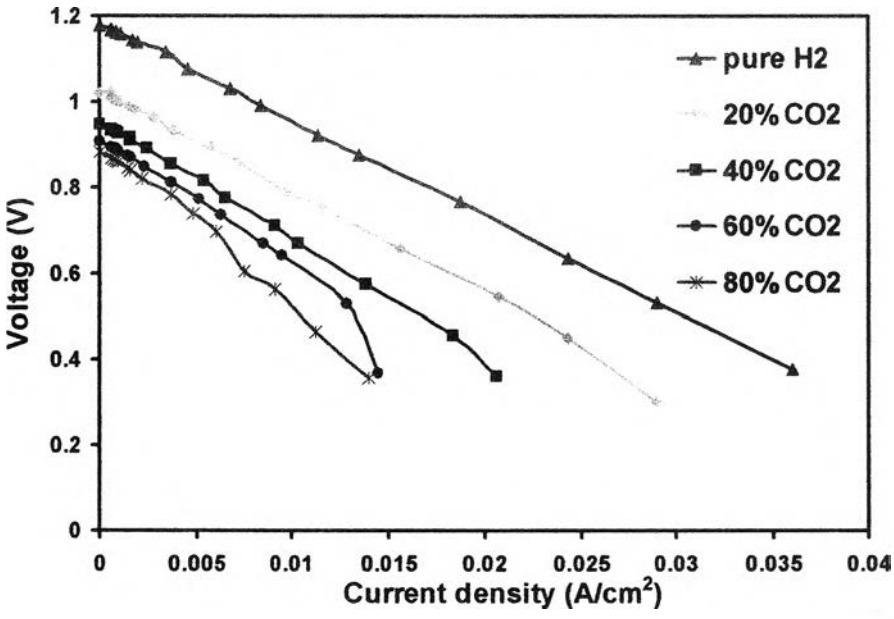

(a)

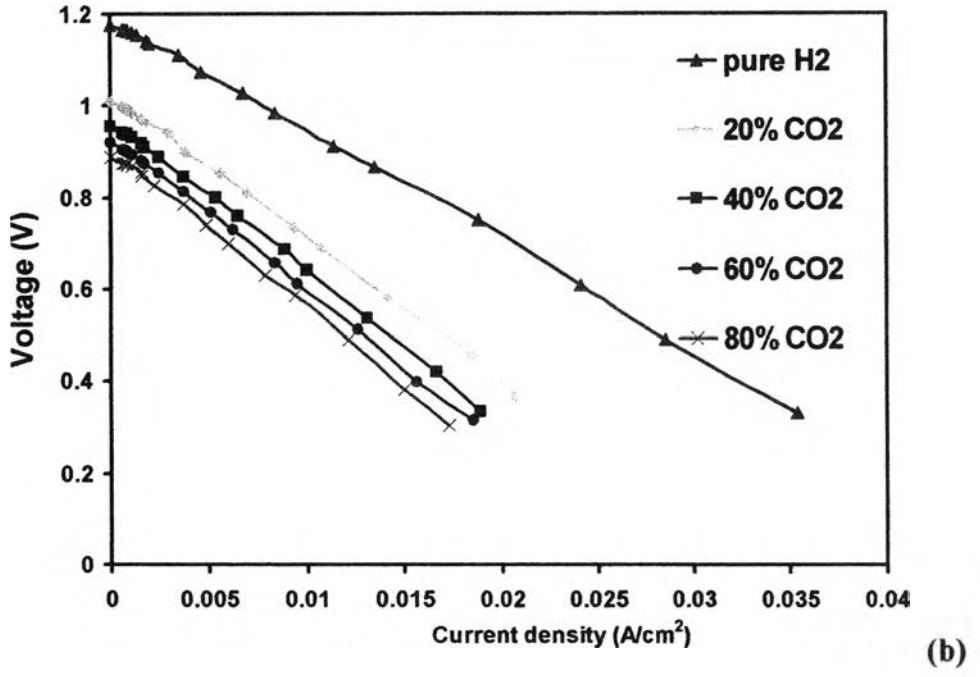

Figure 5.4 Experimental (a) co-flow and (b) counter-flow cell performances using various H_2+CO_2 compositions.

5.5 Effect of H_2/CO Composition

Figures 5.5 (a) and (b) show the cell performances using various H_2+CO compositions for both co- and counter-flows, respectively. H_2+CO compositions were diluted with 50% N_2 to reduce the rate of carbon formation. The results reveal that the impact of CO on OCV and the cell performance is relatively small. OCV decreases about 8% for the co-flow and about 7% for the counter-flow, whereas the cell performance at 0.7 V decreases about 35% and about 31% for the co- and the counter-flows, respectively, when CO content increases up to 80%. This relatively small impact also coincides with simulation results studied by Inui *et al.*, 2006 and experimental results obtained by Suwanwarangkul *et al.*, 2006. A decrease in the cell performance is likely due to a slow rate of CO oxidation which is 2 to 3 times less than H_2 oxidation on Ni-YSZ cermet anode. (Suwanwarangkul. et al, 2006). In contrast with Costa-nunes *et al.*, 2005, they described that Ni was a good CO oxidation catalyst by itself, the lower performance of Ni-YSZ cell for CO fuel cannot be ascribed to poor catalytic activity within the anode. One possible explanation is that the combustion reactions involve fuel molecules adsorbed on the oxide surface at or

near the triple-phase boundary (TPB). Hydrogen adsorbs dissociatively on Ni and it is possible that H atoms "spillover" onto YSZ where oxidation takes place. In contrast to H atoms, spillover of CO adsorbed on a metal to an oxide support generally does not occur.

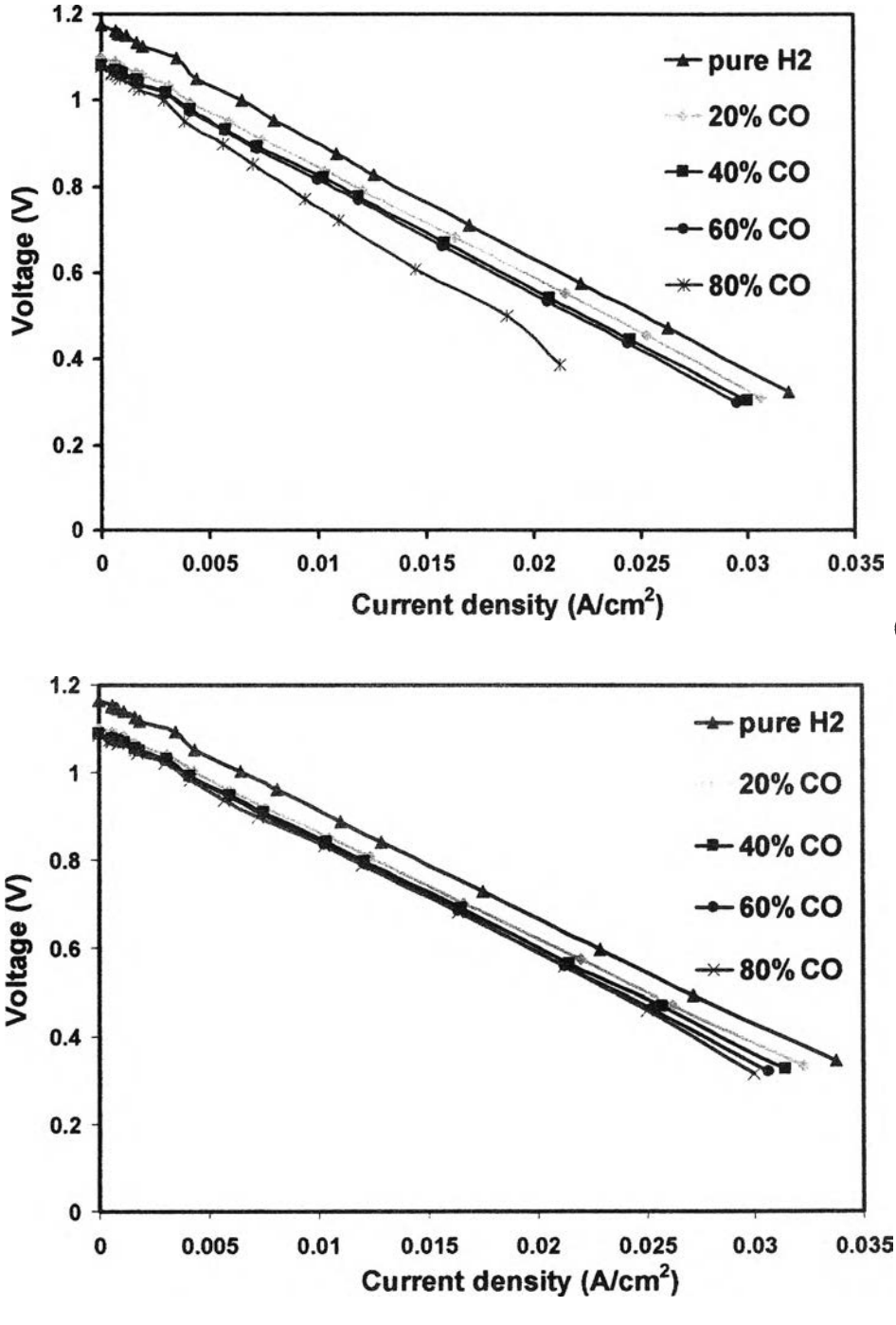

Figure 5.5 Experimental (a) co-flow and (b) counter-flow cell performances using various H_2+CO compositions.

5.6 Effect of Simulated Syngas Composition

Compositions of syngas from literatures, such as bio-oil syngas (Davidian, *et al.*, 2006), biomass syngas (Cordiner *et al.*, 2007), glycerol reformate (Zhang *et al.*, 2006) and coal syngas (Yi *et al.*, 2005) are used as fuels in this case and listed in Table 4. The experimental cell performances using various syngas compositions for both co- and counter-flows are presented in Fig. 5.6 (a) and (b), respectively.

Table 5.1 Compositions of simulated syngas. (% mol, dry basis)

Fuel	$\%H_2$	%CO	$\%CO_2$	$\%N_2$
F1	100	0	0	0
F2	42	0	0	58
F3	42	0	14.25	43.75
F4 Bio-oil syngas	42	18.75	14.25	25
F5 Biomass syngas	42	29.25	3.75	25
F6 Glycerol reformate	51.75	1.5	21.75	25
F7 Coal syngas	27	34.5	13.5	25

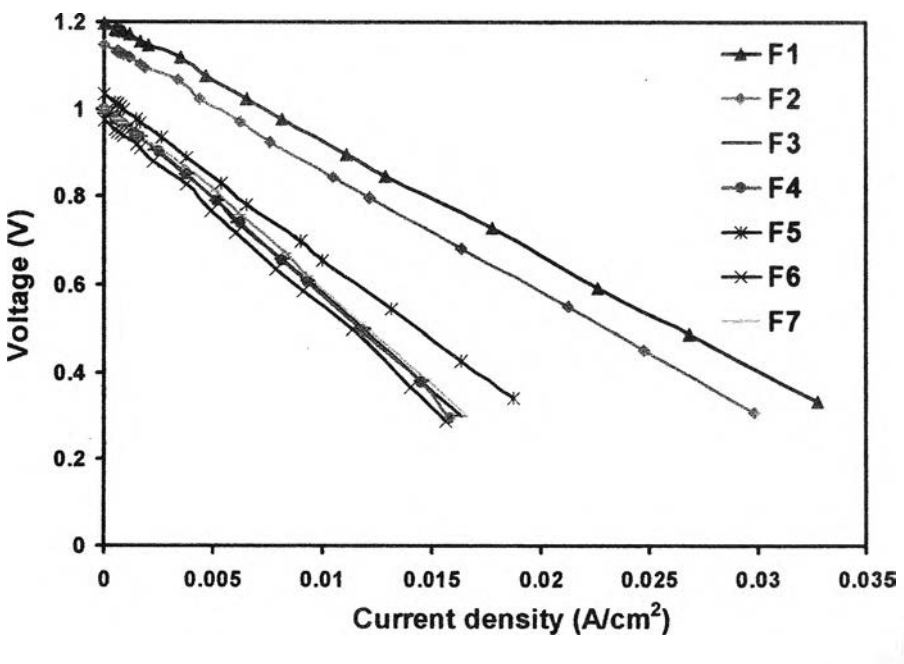

(a)

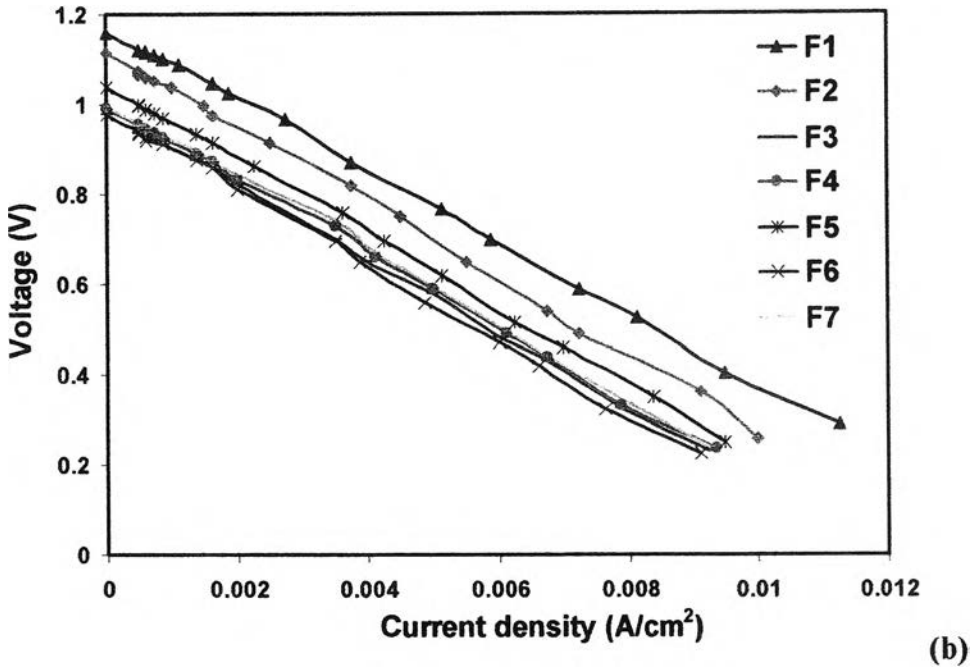

Figure 5.6 Experimental (a) co-flow and (b) counter-flow cell performances using various syngas compositions

As evident from Fig 5.6 (a) and (b), the results reveal that the cell performances using various syngas compositions (F4-F7) are relatively the same. Fuel F1 consisting of pure H_2 provides the highest performance. Interestingly, F4 has a better performance than F3, thus, indicating that the reverse WGS reaction, as mentioned previously, can be suppressed by adding CO to the system. Expectedly, F5 provides a greater performance than F4, F6 and F7 because it contains less CO_2, whereas F7 has a slightly higher performance than F4 due to a slightly lower CO_2 in F7. Finally, even though the highest H_2 content is used, the lowest performance can be obtained when using F6 as a fuel because of its high CO_2 content. Therefore, in the syngas system, it can be concluded that CO_2 has a great impact on the cell performance and if it is removed before the syngas enters into the SOFC, the cell performance could be further increased. On the other hand, the presence of CO_2 helps prevent carbon formation from the Boudouard reaction (Equation 2-5) on the anode. Thus, a trade-off must be made to maximize cell performance and anode durability. (Suwanwarangkul *et al.*, 2006)

5.7 Cell Inspection After Operation

Once an experiment was completed, the electrochemical cell was visually inspected. The anode side of the cell after operation is shown in Fig. 5.7 (a) and (b). As can be seen, the working anode near the fuel outlet shows a slight discoloration which can be explained by a Ni-depletion, while a portion of surface near the fuel inlet was delaminated. A similar phenomenon was reported by Weber *et al.*, 2002.

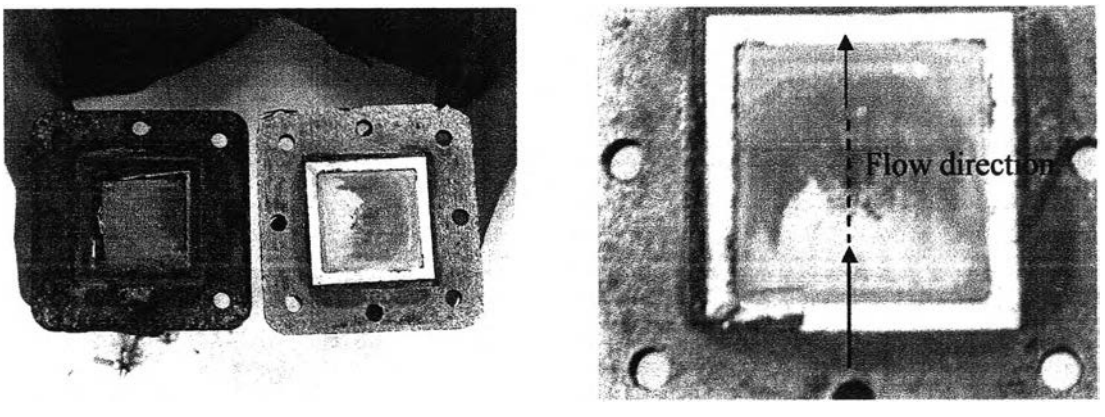

(a) **(b)**

Figure 5.7 Anodic side of the one-cell stack after operation on (a) anode and Pt mesh and (b) anode surface

SEM images of anode surface before and after experiment are presented in Fig. 5.8 (a) and (b), respectively. They are evident that the surface morphologies of the cell after tested significantly differ from that of the fresh cell. This is likely similar to previous reports (Trembly *et al.*, 2006 and Marquez *et al.*, 2007). EDX spectra of anode surface before and after experiment are presented in Fig. 5.9 (a) and (b), respectively. EDX analysis shows a rising of C peak on the anode surface after experiment, confirming that there was C substantially deposits on the anode surface. This may cause performance degradation by one or more mechanism, for example, carbon may block anode pores. Alternatively, the coke buildup may lead to volume expansion and consequent micro-cracking, presumably leading to an interruption of anode current collection pathway (Lin *et al.*, 2005). From our observation, the explanation is that C deposition can occur at 800°C and open-circuit condition which coincides to our operating condition, whereas under close-circuit condition (current

drawing), coking is suppressed by a substantially oxygen ion current and relatively high concentration of reaction products, H_2O and CO_2, within an anode (Lin *et al.*, 2003) which can be written their reactions as follows;

$$C + 2O^{2-} \longrightarrow CO_2 + 4\bar{e} \qquad (5\text{-}1)$$

$$CO_2 + C \longrightarrow 2CO \qquad (5\text{-}2)$$

$$H_2O + C \longrightarrow H_2 + CO \qquad (5\text{-}3)$$

This explanation is supported by the results of the work on direct operation of SOFC with methane where it is found that C deposition does not occur at anode under high current density condition, whereas under low current density condition, substantial deposition is found at a region near the surface only, while a region near the electrolyte is not (Lin *et al.*, 2005).

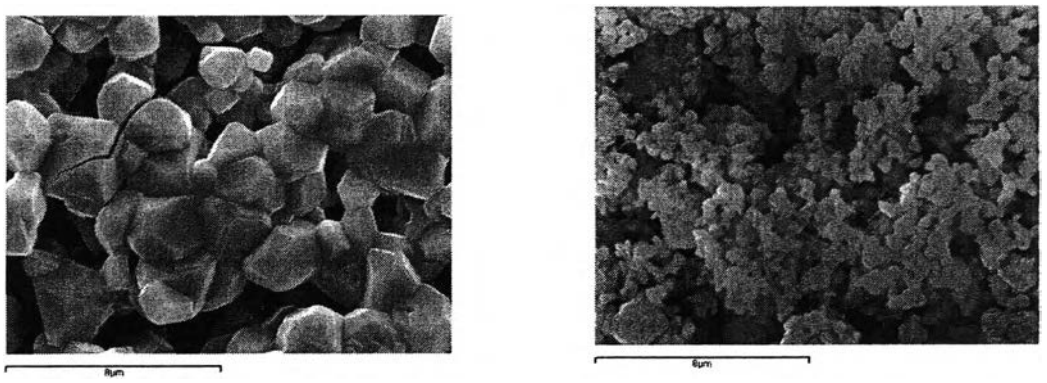

(a) **(b)**

Figure 5.8 SEM images of anode surface of (a) fresh cell and (b) cell after ex periment at 7500 order of magnitude

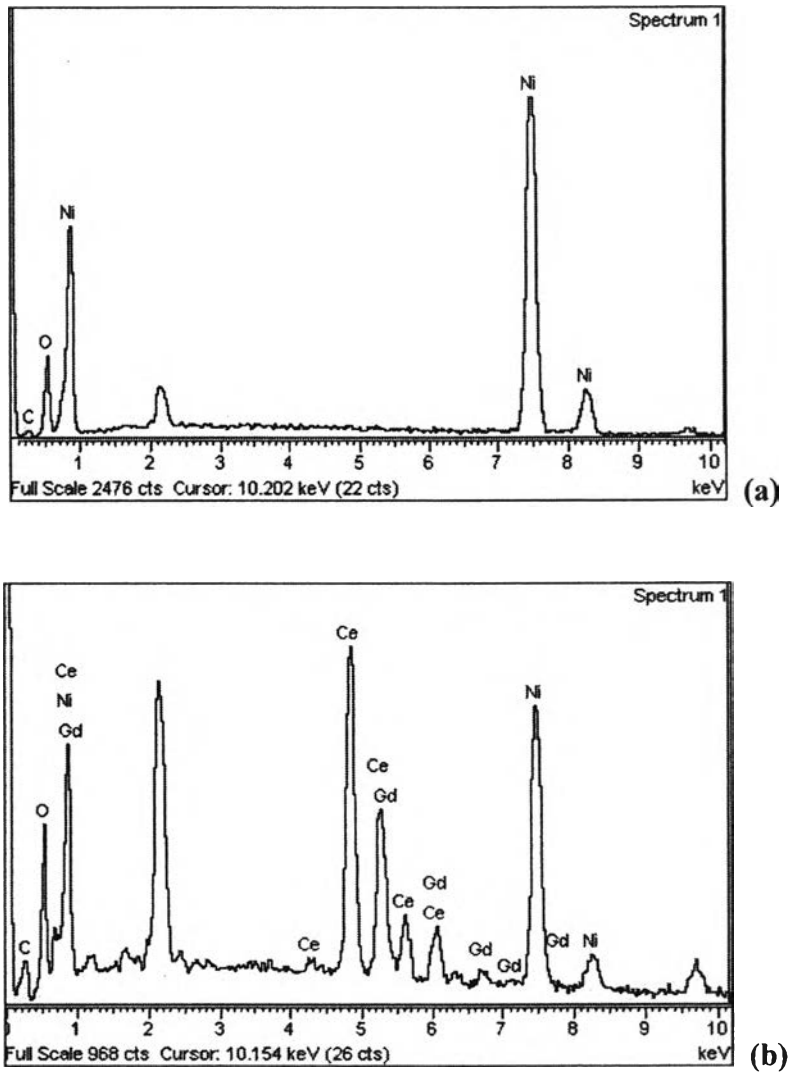

Figure 5.9 EDX spectra of anode surface of (a) a fresh cell and (b) the cell after experiment.

5.8 Modeling and Simulation Results

The cell performances of simulated syngas (F4-F7) for co-flow are presented in Fig. 5.10. As evident, using various syngas compositions, the results show a qualitative agreement (similar trend) with those obtained in the experiment (Fig. 5.6a). It is important to note that since the model is only 2D which neglects the effect of rib width and base on many assumptions, as described in chapter 4, hence, only the trend of the cell performance that model can be predicted, does not give the exact value.

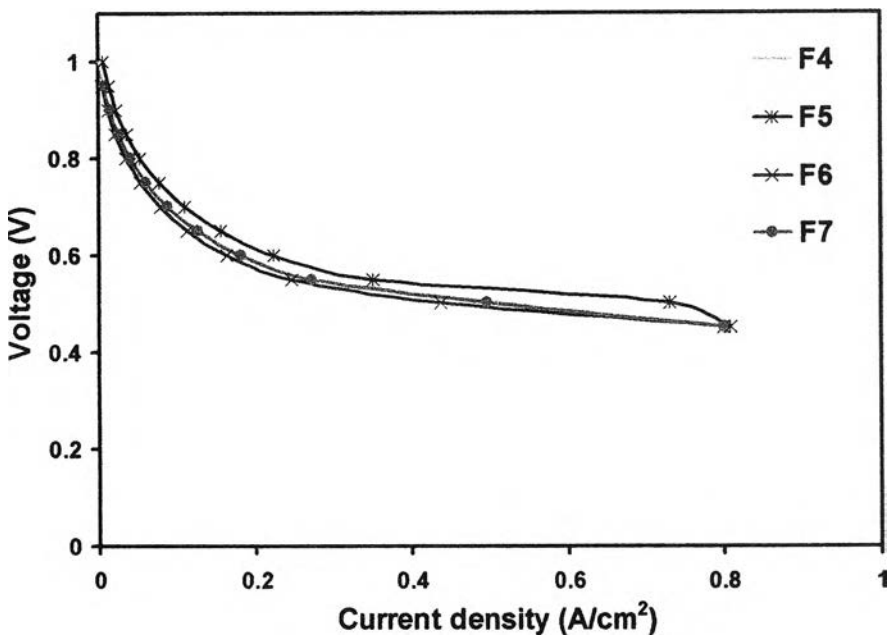

Figure 5.10 The cell performances of simulated syngas for co-flow model.

It is interesting that the cell performances from the experiment are quite different from the model. The former is quite linear which indicates that ohmic polarization is dominant source of the polarization. This may be due to a resistance of transportation of O^{2-} through an electrolyte, and current flow through all stack components. The latter, from the model, is a little curvature. The explanation is that at low current density, activation polarization is dominant and then ohmic polarization is dominating at high current density.

As explained above, one possible way to validate the model is to assume that an electrolyte resistance plays an important role in the cell performance curve. Therefore, model is validated by increasing the electrolyte resistance and fitting with the experimental cell performance for F4. The validated cell performance and the experimental results are compared and illustrated in Fig. 5.11. The results presented the slightly over estimation for F6 and the under estimation for F5.

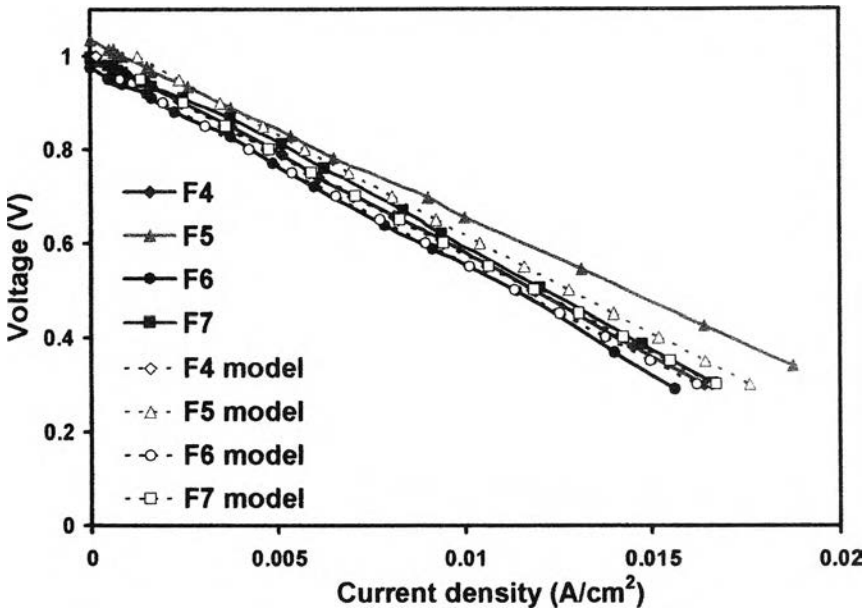

Figure 5.11 Comparison between the experimental cell performances and the validated model cell performance.

From the above results, it has already been demonstrated that the cell performance may not be correctly presented by 2D along the flow channel model. Nonetheless, the overall results still give a good idea of the phenomena occurring in the channel. As a basis of discussion, only one syngas composition is considered and operating condition parameters are listed in Table 5.

Table 5.2 Operating parameters.

Flow configuration	Co-flow
Fuel inlet temperature (K)	1073
Air inlet temperature (K)	1073
Operating pressure (atm)	1
Fuel inlet composition (%)	42 H_2 / 18.75 CO / 14.25 CO_2 / 25 N_2
Air inlet composition (%)	21 O_2 / 79 N_2
Fuel inlet flow rate (mL/min)	200
Air inlet flow rate (mL/min)	100
Cell voltage	0.7, 0.6, 0.5

The distributions of species concentration at the electrolyte/fuel channel interface along the flow channel for the co-flow configuration at 0.7, 0.6 and 0.5 V are illustrated in Fig. 5.12. The profiles present that gas concentration changes rapidly near to the fuel inlet region. This is due to an impact of WGS reaction since at operating temperature, the WGS reaction rate is very fast, therefore; WGS reaction reaches by thermodynamic equilibrium. Since the fuel contains high amount of H_2 and CO_2, WGS reaction thus converts H_2 and CO_2 back to CO and H_2O, resulting in a rapid decrease of H_2 and CO_2 and an increase of CO and H_2O. Once the WGS reaction reaches equilibrium, H_2 and CO are consumed further along the flow channel mainly via electrochemical reactions. The surface plots of fuel and air along the flow channel at 0.5V are illustrated in Fig. 5.13.

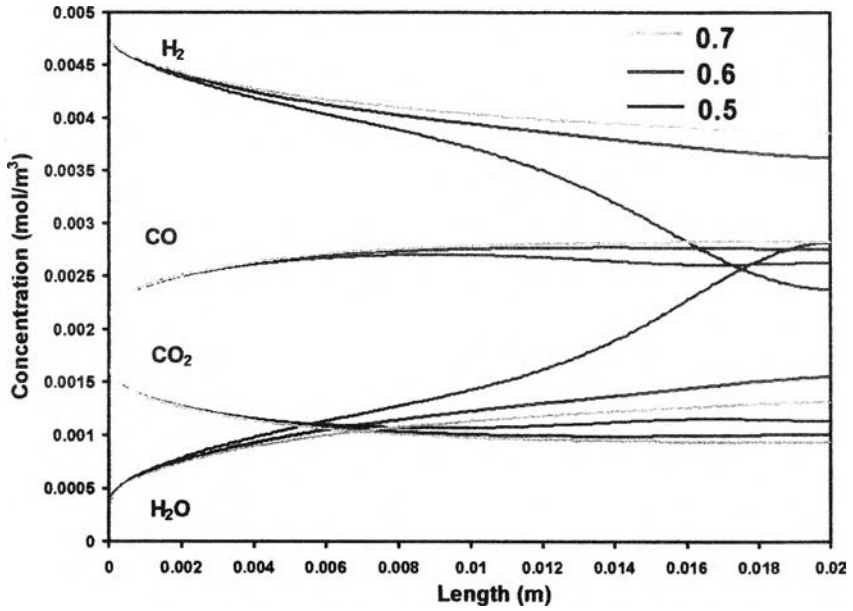

Figure 5.12 Gas concentration at the electrolyte/fuel channel interface at 0.7, 0.6 and 0.5 V.

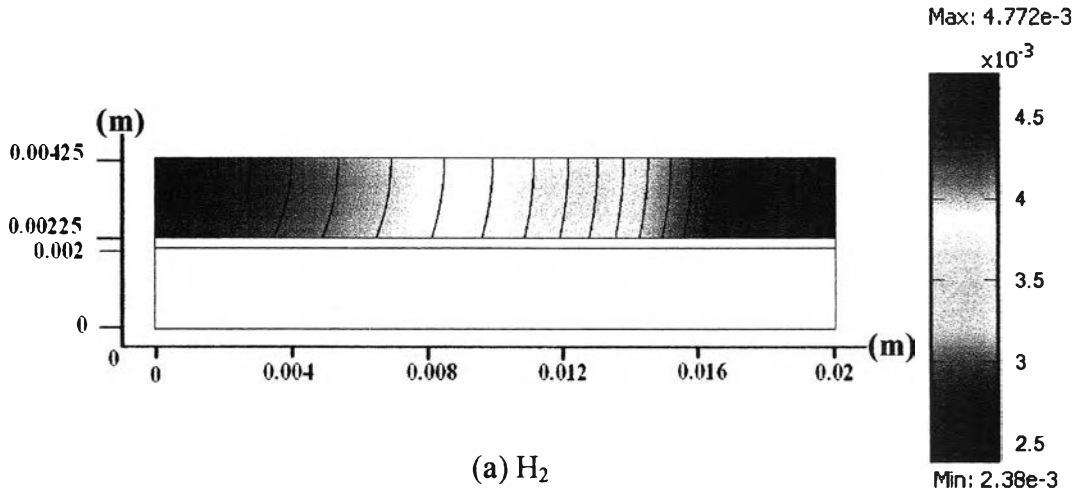
Max: 4.772e-3
x10-3
4.5
4
3.5
3
2.5
Min: 2.38e-3
(m)
0.00425
0.00225
0.002
0
0
0.004
0.008
0.012
0.016
0.02
(m)

(a) H_2

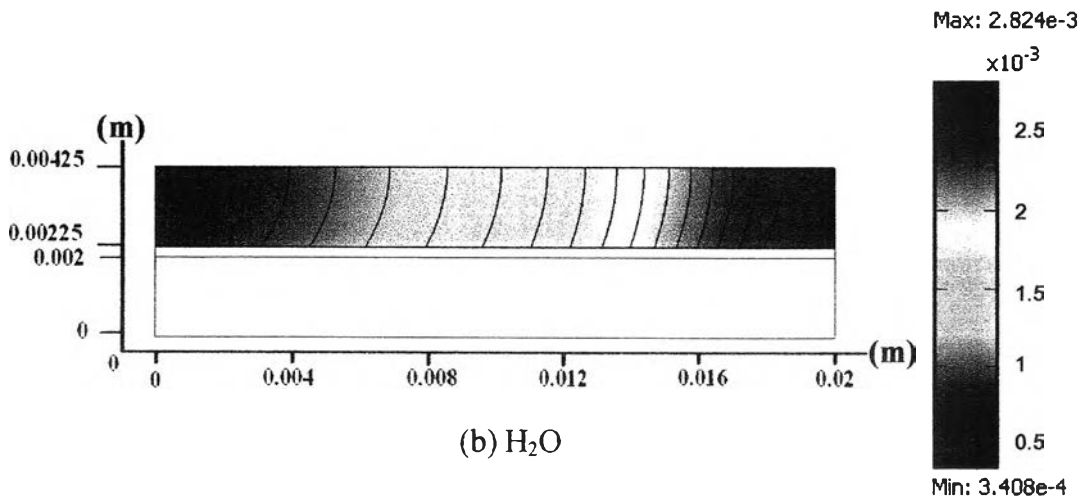
Max: 2.824e-3
x10-3
2.5
2
1.5
1
0.5
Min: 3.408e-4
(m)
0.00425
0.00225
0.002
0
0
0.004
0.008
0.012
0.016
0.02
(m)

(b) H_2O

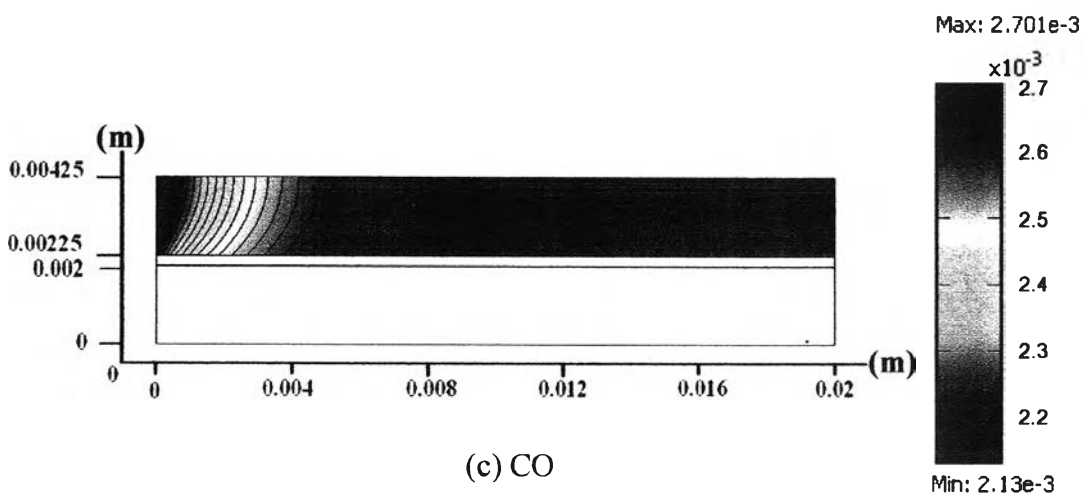
Max: 2.701e-3
x10-3
2.7
2.6
2.5
2.4
2.3
2.2
Min: 2.13e-3
(m)
0.00425
0.00225
0.002
0
0
0.004
0.008
0.012
0.016
0.02
(m)

(c) CO

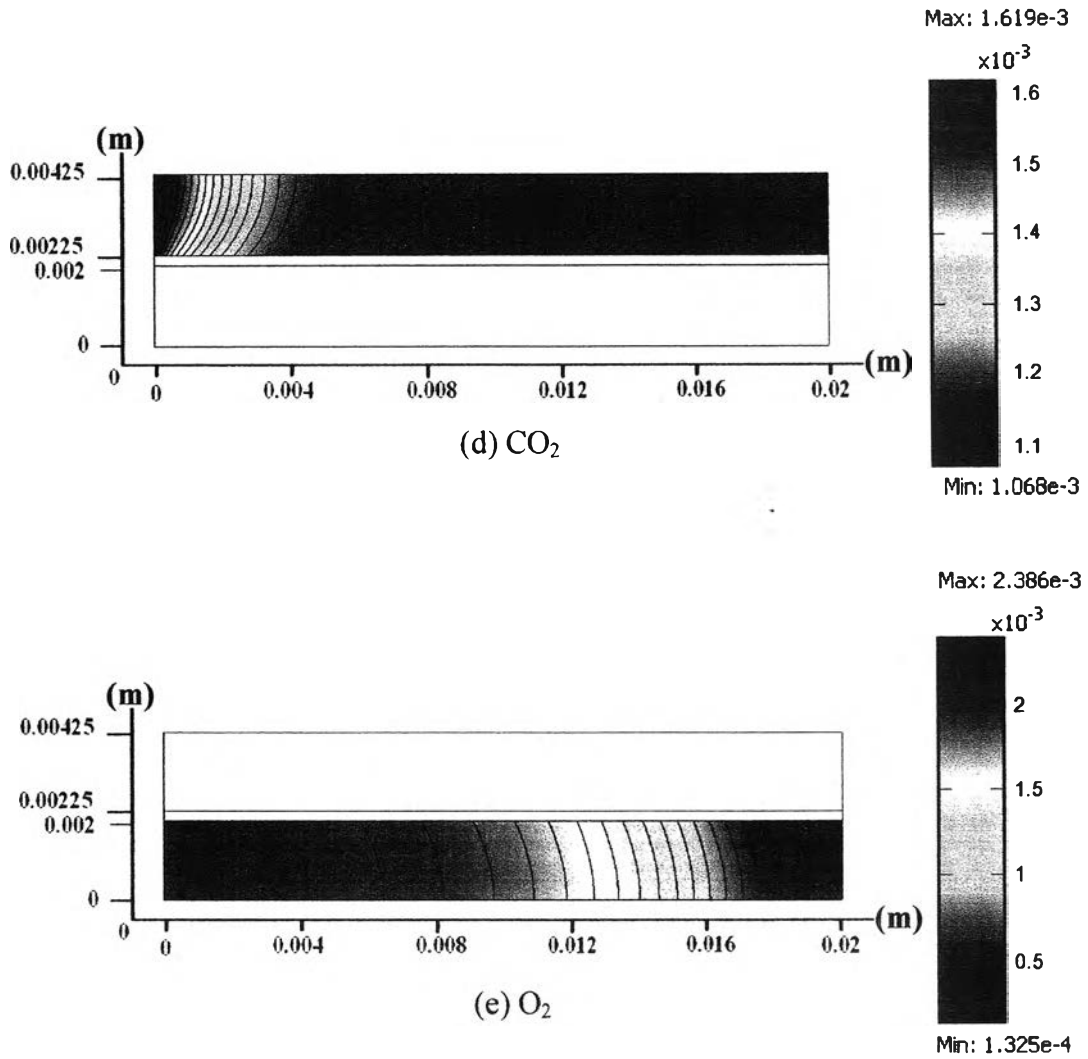

Figure 5.13 Distributions of the concentrations of species (a) H_2, (b) H_2O, (c) CO, (d) CO_2 and (e) O_2

The current density and temperature distributions at the electrolyte/fuel channel interface at 0.7, 0.6 and 0.5V are illustrated in Fig. 5.14 and 5.15, respectively. The results show that at 0.5V, the water-gas shift reaction appreciated at the entrance of the flow channel (length $\leq$ 0.06). As the electrochemical reactions proceed, the temperature start to rapidly increase because of the exothermic of H_2 and CO, and consequently, the current density increase. At the end of the channel, the temperature distribution reaches its maximum value and starts to flatten as a result of a starvation of fuel. A similar report was published on Hernandez-Pacheco *et al.*, 2005. While at

0.6 and 0.7V, current density slightly increases along the flow channel. Therefore, the temperature also slightly increases.

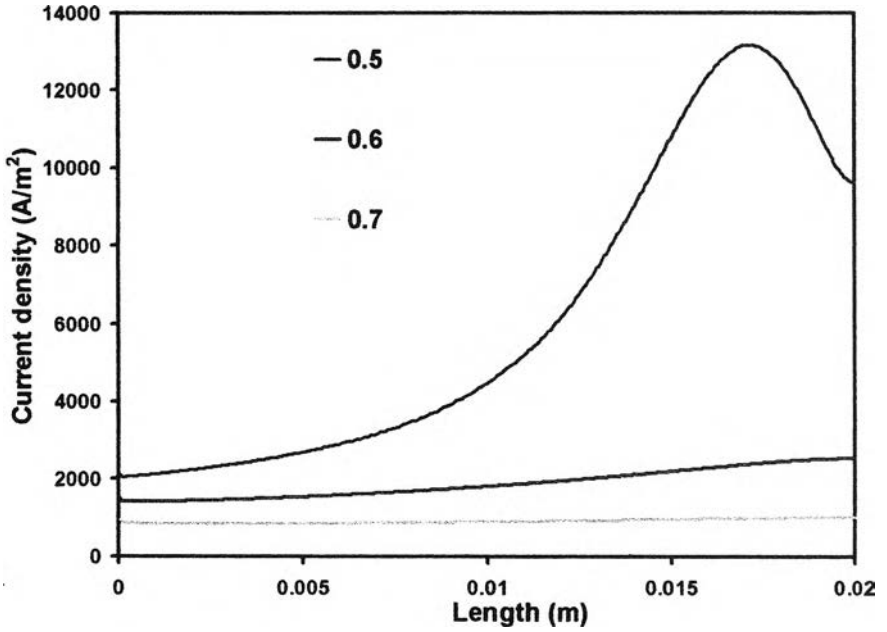

Figure 5.14 Current density distributions at electrolyte/fuel channel interface at 0.7, 0.6 and 0.5V.

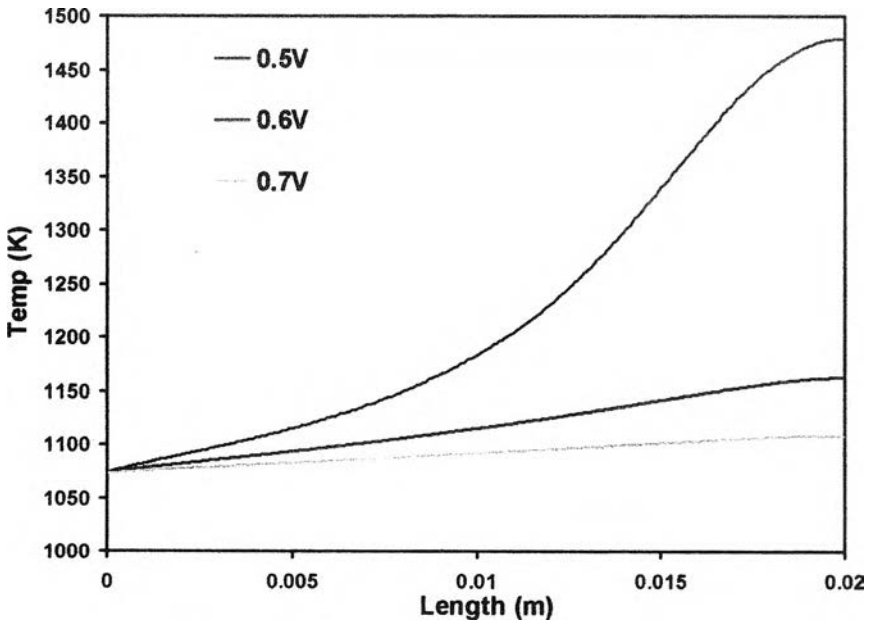

Figure 5.15 Temperature distributions at electrolyte/fuel channel interface at 0.7, 0.6 and 0.5V.

A different approach is taken to explore the possibility to enhance the cell performance of a PSOFC. Since, according to the Butler-Voltmer equation, a current density decreases along the flow channel due to the consumption via electrochemical reaction and production of products, therefore; an evenly distribution of the fuel over the anode surface is required. One possibility in even fuel distribution is used as a "thin-wall" design, as reported in Ramakrishana *et al.*, 2006 that the peak power density was around 35% higher with the thin-wall geometry compared to the normal plain geometry.